Photon antibunching

6

In the previous chapter we studied how light beams can be classified according to their photon statistics. We saw that the observation of Poissonian and super-Poissonian statistics could be explained by classical wave theory, but not sub-Poissonian statistics. Hence sub-Poissonian statistics is a clear signature of the photon nature of light. In this chapter we shall look at a different way of quantifying light according to the second-order correlation function $g^{(2)}(\tau)$. This will lead to an alternative threefold classification in which the light is described as *antibunched*, *coherent*, or *bunched*. We shall see that antibunched light is only possible in the photon interpretation, and is thus another clear signature of the quantum nature of light.

We begin with a classical description of the time-dependent intensity fluctuations in a light beam. These effects were first investigated in detail by R. Hanbury Brown and R. Q. Twiss in the 1950s, and their work has subsequently proven to be of central importance in the development of modern quantum optics. The Hanbury Brown–Twiss (HBT) experiments naturally led to the concept of the second-order correlation function, and we shall study the values that $g^{(2)}(\tau)$ can take for different types of classical light. We shall then see that the quantum theory of light can predict values of $g^{(2)}(\tau)$ that are completely impossible for classical light waves. The light that exhibits these non-classical results is described as being *antibunched*, and is particularly interesting in quantum optics. We conclude with a discussion of the experimental demonstrations of photon antibunching, and the practical application of antibunched light in *single-photon sources*.

This chapter assumes a reasonable familiarity with the coherence properties of light. A short summary of the main points may be found in Section 2.3.

6.1 Introduction: the intensity interferometer

Hanbury Brown and Twiss were astronomers who had a particular interest in measuring the diameters of stars. To this end, they developed the **intensity interferometer** while working at the Jodrell Bank telescope in England. Their interferometer was designed to be an improvement on the Michelson stellar interferometer which was originally implemented on the 2.5 m telescope at Mount Wilson near Los Angeles in the 1920s.

Figure 6.1(a) gives a schematic diagram of the Michelson stellar interferometer. The light from a bright star is collected by two mirrors M_1 and M_2 that are separated by a distance d. The light from each mirror is

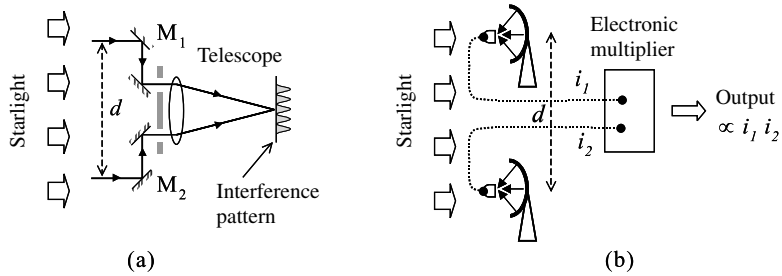

Fig. 6.1 (a) The Michelson stellar interferometer. Coherent light striking the two collection mirrors M_1 and M_2 produces an interference pattern in the focal plane of the telescope. (b) The Hanbury Brown–Twiss (HBT) stellar intensity interferometer. The light recorded on two separated detectors generates photocurrents i_1 and i_2, which are then correlated with each other with an electronic multiplier.

directed through separate slits into the telescope. If the light collected by the two mirrors is coherent, then an interference pattern will be formed in the focal plane of the telescope. On the other hand, if the light is incoherent, no interference pattern will be formed, and the intensities will just add together. The experiment consists in varying d and studying the visibility of the fringes that are observed in the focal plane. An analysis of the variation of the fringe visibility with d enables the angular size of the star to be measured. The actual diameter can then be determined if the star's distance from the earth is known.

We can understand how the Michelson stellar interferometer works by realizing that we are referring to the **spatial coherence** of the starlight, and not its temporal coherence. The spatial coherence is determined by the spread of angles within which light arrives at the interferometer. In an interference experiment, the light arriving at a particular angle generates its own set of bright and dark fringes, but displaced from each other by a distance depending on the angle. (See Exercise 6.1.) If we are not careful, we will have bright fringes for one angle where dark fringes for another angle occur, and vice versa. This would have the effect of washing out the visibility of the fringes, and so it is apparent that interference patterns are only observed when the spread of angles from the source is carefully controlled.

Light from a point source has no angular spread and therefore has perfect spatial coherence. An extended source, on the other hand, delivers light within a finite angular range, and therefore yields only partial spatial coherence.

The angular spread $\delta\theta_s$ of an extended source such as a large star or galaxy is given by:

$$\delta\theta_s = D/L, \tag{6.1}$$

where D is its diameter and L the distance from the earth. This needs to be compared to the diffraction-limited angular resolution of the stellar interferometer $\delta\theta_r$ given by:

$$\delta\theta_r = 1.22\lambda/d, \tag{6.2}$$

where λ is the wavelength of the light and d is the mirror separation. Since d can be larger than the diameter of the telescope optics, the angular resolution is improved compared to the original instrument.

The discussion of the Michelson stellar interferometer given here is somewhat simplified. In particular, the factor of 1.22 in eqn 6.2 is not immediately obvious, given that we are dealing with the diffraction pattern from two mirrors arranged in a line, rather than from a circular aperture. See Brooker (2003) for more details.

On the other hand, the light collection efficiency is worse, because the collection mirrors are usually relatively small. The Michelson stellar interferometer thus improves the angular resolution at the expense of light collection efficiency, and is therefore only useful for observing bright objects.

Let us suppose that we point the stellar interferometer at a small bright star, which acts like a point source in this context with $\delta\theta_s \ll \lambda/d$, for all practical values of d. In these conditions the instrument will not be able to resolve the different angles from the source, and interference fringes will be observed throughout. Now suppose we point the interferometer at an extended source such as a large star or a galaxy so that $\delta\theta_s > 1.22\lambda/d$ for some practical value of d. For $d > 1.22\lambda/\delta\theta_s$, the interferometer will be able to resolve the spread of angles from the source, and the light will be spatially incoherent, so that no interference fringes will be observed. Thus by varying d and recording the fringe visibility, we can determine $\delta\theta_s$, and thus deduce D from eqn 6.1 if L is known.

In the original experiments performed at Mount Wilson in the 1920s, the maximum practical value of d was about 6 m. The angular resolution $\delta\theta_r$ was therefore about 10^{-7} radians for wavelengths in the middle of the visible spectral region with $\lambda \sim 500$ nm. This was sufficient to determine the size of red giants like Betelgeuse in the Orion constellation, which has $\delta\theta_s = 2.2 \times 10^{-7}$ radians. In fact, this was how red giants were discovered.

It is apparent from eqn 6.2 that we need to increase d to improve the angular resolution $\delta\theta_r$ of the stellar interferometer. However, as d get larger, it becomes more and more difficult to hold the collection mirrors steady enough to observe interference fringes. To get around this problem, Hanbury Brown and Twiss proposed the much simpler arrangement shown in Fig. 6.1(b). In their experiment, they used two separated searchlight mirrors to collect light from a chosen star and focused it directly onto separate photomultipliers. This got around the need to form an interference pattern, and made the experiment much easier to perform.

The operating principles of the intensity interferometer will be studied at length in the subsequent sections of this chapter. At this stage we just need to point out that the interferometer measures the correlations between the photocurrents i_1 and i_2 generated by the starlight that impinges on the two photomultipliers. This is done by an electronic multiplying circuit, so that the output of the experiment is proportional to the time average of $i_1 i_2$. This in turn is proportional to $I_1 I_2$, where I_1 and I_2 are the light intensities incident on the two detectors. When d is small, the two detectors collect light from the same area of the source, and hence $I_1(t)$ and $I_2(t)$ will be the same. On the other hand, when d is large, the detectors can differentiate between the light arriving with different angles from the source, so that $I_1(t) \neq I_2(t)$, and the average of $I_1(t)I_2(t)$ will be different. The output of the detector will thus depend on d, and this provides another way of determining the angular spread of the star.

Hanbury Brown and Twiss carried out a series of experiments to test the stellar interferometer during the winter of 1955–6. They demonstrated the validity of their method by obtaining $\delta\theta_s = 3.3\times10^{-8}$ radians for the star Sirius, which was in good agreement with the value determined by other methods. Hanbury Brown then moved to the clearer skies of Australia, where he set up a larger version of the interferometer with d values up to 188 m. The angular resolution of this improved instrument was 2×10^{-9} radians, which led to the measurement of the diameters of several hundreds of the brighter stars for the first time.

See R. Hanbury Brown and R. Q. Twiss, *Nature* **178**, 1046 (1957). The comment made above about the Michelson stellar interferometer sacrificing sensitivity for resolution applies even more strongly to the intensity interferometer. The latter is typically several orders of magnitude less sensitive.

In the context of this present work on quantum optics, the interest in the HBT experiments is in the interpretation of the results. We have mentioned above that the interferometer measures *correlations* between the light intensities recorded by two separated photodetectors. This raises many conceptual difficulties. If each individual photodetection event is a statistical quantum process, how can separated events be correlated with each other?

The conceptual difficulty can be resolved by taking a semi-classical approach, such as the one taken in Section 5.8.1, in which the light is treated classically, and quantum theory is only introduced in the photodetection process itself. This approach was enough to satisfy the original critics of the HBT experiments. However, it transpires that if we really treat the light as a quantum object, then the objections raised are perfectly valid. In fact, the quantum theory of light predicts results in HBT experiments that are impossible for classical light. The aim of this chapter is to explain how these quantum optical effects can be observed and to describe the sources that produce them. Before we do this, however, we first review the classical theory of the HBT experiments.

The original experiments of Hanbury Brown and Twiss did not reveal any quantum optical effects because single-photon detectors with high quantum efficiencies were not available and they were looking at the thermal light from stars and galaxies. It was not until the 1970s that detectors of sufficient efficiency and new types of light sources were available to demonstrate the purely quantum optical effects.

6.2 Hanbury Brown–Twiss experiments and classical intensity fluctuations

Hanbury Brown and Twiss realized that their stellar interferometer was raising conceptual difficulties, and so they decided to test the principles of their experiment in the laboratory with the simpler arrangement shown in Fig. 6.2. In this experiment the 435.8 nm line from a mercury discharge lamp was split by a half-silvered mirror and then detected by two small photomultipliers PMT1 and PMT2, generating photocurrents i_1 and i_2, respectively. These photocurrents were then fed into AC-coupled amplifiers, which gave outputs proportional to the fluctuations in the photocurrents, namely Δi_1 and Δi_2. One of these was passed through an electronic time delay generator set to a value τ. Finally, the two signals were connected to a multiplier–integrator unit which multiplied them together and averaged them over a long time. The final output signal was thus proportional to $\langle \Delta i_1(t)\Delta i_2(t+\tau)\rangle$, where the symbol $\langle\cdots\rangle$ indicates the time average. Since the photocurrents were proportional to the impinging light intensities, it is apparent that the

The original HBT experiment is described in *Nature*, **177**, 27 (1956). Hanbury Brown and Twiss subsequently gave more detailed accounts in *Proc. Roy. Soc. A* **242**, 300 (1957) and **243**, 291 (1958). AC coupling was used so that the large DC photocurrent from the detectors and the electrical $1/f$ noise did not saturate the high-gain amplifiers. *RC* filters were used to block the low frequencies, and only the fluctuations in the frequency range 3–27 MHz were amplified.

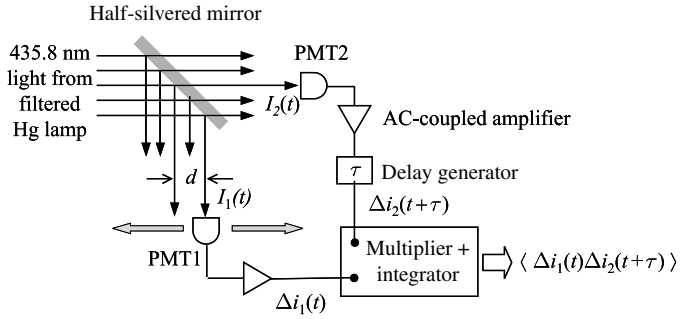

Fig. 6.2 Schematic representation of the Hanbury Brown–Twiss (HBT) intensity correlation experiment. The light from a mercury lamp was filtered so that only the 435.8 nm emission line impinged on a half-silvered mirror. Two photomultipliers tubes PMT1 and PMT2 detected the reflected and transmitted light intensities $I_1(t)$ and $I_2(t)$, respectively. The photocurrent signals generated by the detectors were filtered and amplified, and one of them was delayed by a time τ. The two amplified photocurrent fluctuation signals $\Delta i_1(t)$ and $\Delta i_2(t+\tau)$ were then fed into an electronic multiplier–integrator, giving an output proportional to $\langle \Delta i_1(t)\Delta i_2(t+\tau)\rangle$. PMT1 was placed on a translation stage, so that the two detectors could register light separated by a distance d. In this way, the spatial coherence of the source could be investigated. (After R. Hanbury Brown and R.Q. Twiss, *Nature*, **177**, 27 (1956).)

output was in fact proportional to $\langle \Delta I_1(t)\Delta I_2(t+\tau)\rangle$, where $I_1(t)$ and $I_2(t)$ were the light intensities incident on the respective detectors, and ΔI_1 and ΔI_2 were their fluctuations.

The light emitted by a mercury lamp originates from many different atoms. This leads to fluctuations in the light intensity on time-scales comparable to the coherence time, τ_c. These light intensity fluctuations originate from fluctuations in the numbers of atoms emitting at a given time, and also from jumps and discontinuities in the phase emitted by the individual atoms. The partially coherent light emitted from such a source is called **chaotic** to emphasize the underlying randomness of the emission process at the microscopic level.

See Section 5.5.2 for further discussion of chaotic light.

Figure 6.3 shows a computer simulation of the time dependence of the intensity of the light emitted by a chaotic source with a coherence time of τ_c. It is apparent that the intensity fluctuates wildly above and below the average value $\langle I\rangle$ on time-scales comparable to τ_c. These intensity fluctuations are caused by the addition of the randomly phased light from the millions of light-emitting atoms in the source. We suppose that each atom emits at the same frequency, but that the phase of the light from the individual atoms is constantly changing due to the random collisions.

A typical collision-broadened discharge lamp will have a spectral width $\Delta\nu \sim 10^9$ Hz, so that from eqn 2.41 we expect $\tau_c \sim 1$ ns.

The principle behind the HBT experiments is that the intensity fluctuations of a beam of light are related to its coherence. If the light impinging on the two detectors is coherent, then the intensity fluctuations will be *correlated* with each other. Thus by measuring the correlations of the intensity fluctuations, we can deduce the coherence

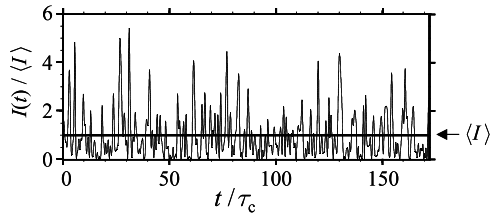

Fig. 6.3 Computer simulation of the time dependence of the light intensity emitted by a chaotic source with a coherence time of τ_c and average intensity $\langle I \rangle$. (After A.J. Bain and A. Squire, *Opt. Commun.* **135**, 157 (1997), © Elsevier, reproduced with permission.)

properties of the light. This is much easier than setting up interference experiments, and gives us other insights as well.

Consider the results of the HBT experiment shown in Fig. 6.2 with d set at zero. We adjust the beam splitter so that the average intensity $\langle I(t) \rangle$ impinging on the detectors is identical. From a classical perspective, we can write the time-varying light intensity on the detectors as:

$$I_1(t) = I_2(t) \equiv I(t) = \langle I \rangle + \Delta I(t). \tag{6.3}$$

where $2I(t)$ is the intensity incident on the beam splitter and $\Delta I(t)$ is the fluctuation from the mean intensity $\langle I \rangle$. With identical intensities on the detectors, the output of the HBT experiment is proportional to $\langle \Delta I(t) \Delta I(t+\tau) \rangle$.

Let us suppose that we set the time delay τ to be zero. The output is then:

$$\langle \Delta I(t) \Delta I(t+\tau) \rangle_{\tau=0} = \langle \Delta I(t)^2 \rangle. \tag{6.4}$$

Although $\langle \Delta I(t) \rangle$ is equal to zero by definition, $\langle \Delta I(t)^2 \rangle$ will be non-zero due to the intensity fluctuations in the chaotic light from the discharge lamp. Hence there will be a non-zero output for $\tau = 0$. On the other hand, if we make $\tau \gg \tau_c$, the intensity fluctuations will be completely uncorrelated with each other, so that $\Delta I(t) \Delta I(t+\tau)$ randomly changes sign with time and averages to zero:

$$\langle \Delta I(t) \Delta I(t+\tau) \rangle_{\tau \gg \tau_c} = 0. \tag{6.5}$$

The output therefore falls to zero for values of $\tau \gg \tau_c$. Hence by measuring the output as a function of τ, we can determine τ_c directly.

In their original experiments, Hanbury Brown and Twiss set $\tau = 0$ and varied d. As d increased, the spatial coherence of the light impinging on the two detectors decreased. Hence the correlations between ΔI_1 and ΔI_2 eventually vanished for large values of d, and the output fell to zero. Their method therefore provided a way to determine the spatial coherence of the source through the decreased intensity correlations at large d values. The stellar intensity interferometer works by the same principle.

We have been assuming throughout this discussion that the detector can respond to the fast fluctuations in the light intensity on time-scales comparable to the coherence time τ_c. This requires very fast detectors that were not available in the 1950s. If the response time of the detector τ_D is longer than τ_c, it can be shown that the signal at $\tau = 0$ is reduced by a factor (τ_c/τ_D). See, for example, Loudon (2000, §3.8), or Mandel and Wolf (1995, §14.7.1.) Therefore, when $\tau_D > \tau_c$, we still expect the experiment to work and the output to fall to zero on a time-scale $\sim \tau_c$, although it becomes more difficult to observe the effect due to the smaller size of the signal.

6.3 The second-order correlation function $g^{(2)}(\tau)$

In the previous section we considered how the results of the HBT experiments can be explained classically in terms of intensity correlations. In order to analyse these results in a quantifiable way, it is helpful to introduce the **second-order correlation function** of the light defined by:

$$g^{(2)}(\tau) = \frac{\langle \mathcal{E}^*(t)\mathcal{E}^*(t+\tau)\mathcal{E}(t+\tau)\mathcal{E}(t)\rangle}{\langle \mathcal{E}^*(t)\mathcal{E}(t)\rangle\langle \mathcal{E}^*(t+\tau)\mathcal{E}(t+\tau)\rangle} = \frac{\langle I(t)I(t+\tau)\rangle}{\langle I(t)\rangle\langle I(t+\tau)\rangle}, \qquad (6.6)$$

where $\mathcal{E}(t)$ and $I(t)$ are the electric field and intensity of the light beam at time t. The $\langle\cdots\rangle$ symbols again indicate the time average computed by integrating over a long time period.

The second-order correlation function $g^{(2)}(\tau)$ is the intensity analogue of the first-order correlation function $g^{(1)}(\tau)$ that determines the visibility of interference fringes. (See Section 2.3.) By comparing eqns 2.42 and 6.6, we can see that $g^{(1)}(\tau)$ quantifies the way in which the electric field fluctuates in time, whereas $g^{(2)}(\tau)$ quantifies the intensity fluctuations. In classical optics texts, $g^{(2)}(\tau)$ is often called the **degree of second-order coherence**.

Let us consider a source with constant average intensity such that $\langle I(t)\rangle = \langle I(t+\tau)\rangle$. We shall also assume from now on that we are testing the spatially coherent light from a small area of the source. In these circumstances the second-order correlation function investigates the *temporal* coherence of the source.

We have seen above that the time-scale of the intensity fluctuations is determined by the coherence time τ_c of the source. If $\tau \gg \tau_c$, the intensity fluctuations at times t and $t+\tau$ will be completely uncorrelated with each other. On writing

$$I(t) = \langle I\rangle + \Delta I(t) \qquad (6.7)$$

as before, with $\langle \Delta I(t)\rangle = 0$, we then have from eqn 6.5 that:

$$\begin{aligned}\langle I(t)I(t+\tau)\rangle_{\tau\gg\tau_c} &= \Big\langle \left(\langle I\rangle + \Delta I(t)\right)\left(\langle I\rangle + \Delta I(t+\tau)\right)\Big\rangle \\ &= \langle I\rangle^2 + \langle I\rangle\langle \Delta I(t)\rangle + \langle I\rangle\langle \Delta I(t+\tau)\rangle \\ &\quad + \langle \Delta I(t)\Delta I(t+\tau)\rangle \\ &= \langle I\rangle^2. \end{aligned} \qquad (6.8)$$

It is therefore apparent that:

$$g^{(2)}(\tau \gg \tau_c) = \frac{\langle I(t)I(t+\tau)\rangle}{\langle I(t)\rangle^2} = \frac{\langle I(t)\rangle^2}{\langle I(t)\rangle^2} = 1. \qquad (6.9)$$

On the other hand, if $\tau \ll \tau_c$, there will be correlations between the fluctuations at the two times. In particular, if $\tau = 0$, we have

$$g^{(2)}(0) = \frac{\langle I(t)^2\rangle}{\langle I(t)\rangle^2}. \qquad (6.10)$$

It can be shown that for any conceivable time dependence of $I(t)$, it will always be the case that

$$g^{(2)}(0) \geq 1, \qquad (6.11)$$

and

$$g^{(2)}(0) \geq g^{(2)}(\tau). \qquad (6.12)$$

These results can be proven rigorously (see Exercises 6.3 and 6.4), but we can also give a simple intuitive explanation of why they must apply.

Consider first a perfectly coherent monochromatic source with a time-independent intensity I_0. In this case, it is trivial to see that:

$$g^{(2)}(\tau) = \frac{\langle I(t)I(t+\tau)\rangle}{\langle I(t)\rangle^2} = \frac{I_0^2}{I_0^2} = 1, \tag{6.13}$$

for all values of τ, because I_0 is a constant. Next, recall that we expect from eqn 6.9 that $g^{(2)}(\tau) = 1$ for all large values of τ. Finally consider any source with a time-varying intensity. It is apparent that $\langle I(t)^2\rangle > \langle I(t)\rangle^2$ because there are equal intensity fluctuations above and below the average, and the squaring process exaggerates the fluctuations above the mean value. (See Example 6.1 below.) On using this fact in eqn 6.10, we see that we must have $g^{(2)}(0) > 1$. Putting it all together, we realize that, for any source with a time-varying intensity, we expect $g^{(2)}(\tau)$ to decrease with τ, reaching the value of unity for large τ. In the special case where $I(t)$ does not vary with time, we expect a constant value of $g^{(2)}(\tau) = 1$. These conclusions concur with the rigorous results given in eqns 6.11 and 6.12.

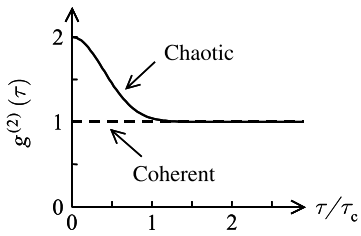

Fig. 6.4 Second-order correlation function $g^{(2)}(\tau)$ for chaotic and perfectly coherent light plotted on the same time-scale. The chaotic light is assumed to be Doppler-broadened with a coherence time of τ_c.

It is instructive to consider the explicit forms of the second-order correlation function for the various forms of light that we usually consider in classical optics. We have already seen that perfectly coherent light has $g^{(2)}(\tau) = 1$ for all τ. The values of $g^{(2)}(\tau)$ for the chaotic light from an atomic discharge lamp can be calculated by assuming simple models of the source. If the spectral line is Doppler-broadened with a Gaussian lineshape, the second-order correlation function is given by:

$$g^{(2)}(\tau) = 1 + \exp\left[-\pi(\tau/\tau_c)^2\right]. \tag{6.14}$$

This function is plotted in Fig. 6.4 and compared to that of perfectly coherent light. Similarly, a lifetime-broadened source with a Lorentzian lineshape has a $g^{(2)}$ function given by:

$$g^{(2)}(\tau) = 1 + \exp\left(-2|\tau|/\tau_0\right), \tag{6.15}$$

where τ_0 is the radiative lifetime for the spectral transition, or the collision time, as appropriate.

The main properties of the second-order correlation function $g^{(2)}(\tau)$ are listed in Table 6.1. These properties are derived by assuming that the

The derivations of eqns 6.14 and 6.15 may be found, for example, in Loudon (2000, §3.7). Note that both Doppler and Lorentzian-broadened chaotic light have $g^{(2)}(0) = 2$, with the value of $g^{(2)}(\tau)$ decreasing towards unity for $\tau \gg \tau_c$. Hence they both satisfy the general conditions set out in eqns 6.11 and 6.12.

Table 6.1 Properties of the second-order correlation function $g^{(2)}(\tau)$ for classical light.

Light source	Property	Comment
All classical light	$g^{(2)}(0) \geq 1$ $g^{(2)}(0) \geq g^{(2)}(\tau)$	$g^{(2)}(0) = 1$ when $I(t) =$ constant
Perfectly coherent light	$g^{(2)}(\tau) = 1$	Applies for all τ
Gaussian chaotic light	$g^{(2)}(\tau) = 1 + \exp\left[-\pi(\tau/\tau_c)^2\right]$	τ_c = coherence time
Lorentzian chaotic light	$g^{(2)}(\tau) = 1 + \exp\left(-2\lvert\tau\rvert/\tau_0\right)$	τ_0 = lifetime

light consists of classical electromagnetic waves. In the sections below we shall reconsider the HBT experiments with photons incident on the beam splitter rather than classical light waves. We shall find that the two conditions given in eqns 6.11 and 6.12 do not necessarily have to be obeyed. In particular, we shall see that it is possible to have light with $g^{(2)}(0) < 1$, in violation of the classical result given in eqn 6.11. The observation of $g^{(2)}(0) < 1$ is thus a conclusive signature of the quantum nature of light.

Example 6.1 Evaluate $g^{(2)}(0)$ for a monochromatic light wave with a sinusoidal intensity modulation such that $I(t) = I_0(1 + A\sin\omega t)$ with $|A| \leq 1$.

Solution
We compute $g^{(2)}(0)$ from eqn 6.10 according to:

$$g^{(2)}(0) = \frac{\langle I(t)^2\rangle}{\langle I(t)\rangle^2} = \frac{\langle I_0^2(1 + A\sin\omega t)^2\rangle}{I_0^2} = \langle(1 + A\sin\omega t)^2\rangle,$$

where we used $\langle I(t)\rangle = I_0\langle(1 + A\sin\omega t)\rangle = I_0$ since $\langle\sin\omega t\rangle = 0$. We compute the time average by taking the integral over a long time interval T, with $T \gg 1/\omega$:

$$\begin{aligned} g^{(2)}(0) &= (1/T)\int_0^T (1 + A\sin\omega t)^2\,\mathrm{d}t \\ &= (1/T)\int_0^T (1 + 2A\sin\omega t + A^2\sin^2\omega t)\,\mathrm{d}t. \end{aligned}$$

On using $2\sin^2 x = (1 - \cos 2x)$, and with both $\sin\omega t$ and $\cos 2\omega t$ averaging to zero, this then gives:

$$g^{(2)}(0) = 1 + \frac{A^2}{2T}\int_0^T (1 - \cos 2\omega t)\mathrm{d}t = 1 + A^2/2.$$

$g^{(2)}(0)$ is therefore always greater than unity, and its maximum value is equal to 1.5 for $|A| = 1$.

6.4 Hanbury Brown–Twiss experiments with photons

The quantum theory of the HBT experiment will be given in Section 8.5. We restrict ourselves here to a qualitative understanding of the experiments and the classification of light according to the second-order correlation function that naturally emerges from the analysis.

It is now time to re-examine the Hanbury Brown–Twiss (HBT) experiment in the quantum picture of light. Figure 6.5(a) illustrates the experimental arrangement for a HBT experiment configured with single-photon counting detectors. A stream of photons is incident on a 50 : 50 beam splitter, and is divided equally between the two output ports. The photons impinge on the detectors and the resulting output pulses are fed into an electronic counter/timer. The counter/timer records the time that elapses between the pulses from D1 and D2, while simultaneously

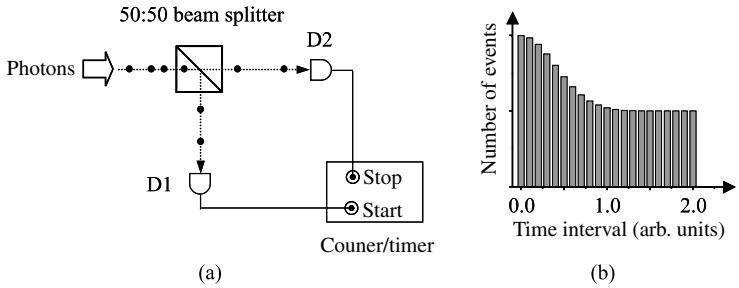

Fig. 6.5 (a) Hanbury Brown–Twiss (HBT) experiment with a photon stream incident on the beam splitter. The pulses from the single-photon counting detectors D1 and D2 are fed into the start and stop inputs of an electronic counter/timer. The counter/timer both counts the number of pulses from each detector and also records the time that elapses between the pulses at the start and stop inputs. (b) Typical results of such an experiment. The results are presented as a histogram showing the number of events recorded within a particular time interval. In this case the histogram shows the results that would be obtained for a bunched photon stream.

counting the number of pulses at each input. The results of the experiment are typically presented as a histogram, as shown in Fig. 6.5(b). The histogram displays the number of events that are registered at each value of the time τ between the start and stop pulses.

In Section 6.3 we discussed the $g^{(2)}(\tau)$ function classically in terms of intensity correlations. Since the number of counts registered on a photon-counting detector is proportional to the intensity (cf. eqn 5.2), we can rewrite the classical definition of $g^{(2)}(\tau)$ given in eqn 6.6 as:

$$g^{(2)}(\tau) = \frac{\langle n_1(t) n_2(t+\tau)\rangle}{\langle n_1(t)\rangle \langle n_2(t+\tau)\rangle}, \tag{6.16}$$

where $n_i(t)$ is the number of counts registered on detector i at time t. This shows that $g^{(2)}(\tau)$ is dependent on the simultaneous probability of counting photons at time t on D1 and at time $t+\tau$ on D2. In other words, $g^{(2)}(\tau)$ is proportional to the conditional probability of detecting a second photon at time $t=\tau$, given that we detected one at $t=0$. This is exactly what the histogram from the HBT experiment with photon-counting detectors records. Hence the results of the HBT experiment also give a direct measure of the second-order correlation function $g^{(2)}(\tau)$ in the photon interpretation of light.

A moment's thought makes us realize that completely different results are possible with photons at the input port of the beam splitter than with a classical electromagnetic wave. Let us suppose that the incoming light consists of a stream of photons with long time intervals between successive photons. The photons then impinge on the beam splitter one by one and are randomly directed to either D1 or D2 with equal probability. There is therefore a 50% probability that a given photon will be detected by D1 and trigger the timer to start recording. The generation of a start pulse in D1 implies that there is a zero probability of obtaining a stop pulse from D2 from this photon. Hence the timer will record no events at $\tau = 0$. Now consider the next photon that impinges on the

The correct normalization of $g^{(2)}(\tau)$ is very important for establishing non-classical results with $g^{(2)}(0) < 1$. The counter/timer arrangement shown in Fig. 6.5 produces a histogram that is proportional to $g^{(2)}(\tau)$ but does not give its exact value. From an experimental point of view, the normalization can be performed by assuming that $g^{(2)}(\tau) = 1$ for very long time delays. Alternatively, the non-classical source can be replaced by a Poissonian source of the same average intensity and the coincidence rates compared. Single-mode laser light can serve as a convenient Poissonian calibration source.

We are, of course, assuming here that the detectors have unity quantum efficiencies. Less perfect detectors would reduce the overall count rate, but would not affect the essential gist of the argument.

beam splitter. This will go to D2 with probability 50%, and if it does so, it will stop the timer and record an event. If the photon goes to D1, then nothing happens and we have to wait again until the next photon arrives to get a chance of having a stop pulse. The process proceeds until a stop pulse is eventually achieved. This might happen with the first or second or any subsequent photon, but never at $\tau = 0$. We therefore have a situation where we expect no events at $\tau = 0$, but some events for larger values of τ, which clearly contravenes the classical result given in eqns 6.11 and 6.12. We thus immediately see that the experiment with photons can give results that are not possible in the classical theory of light.

The observation of the non-classical result with $g^{(2)}(0) = 0$ arose from the fact that the photon stream consisted of individual photons with long time intervals between them. Let us now consider a different scenario in which the photons arrive in bunches. Half of the photons are split towards D1 and the other half towards D2. These two subdivided bunches strike the detectors at the same time and there will be a high probability that both detectors register simultaneously. There will therefore be a large number of events near $\tau = 0$. On the other hand, as τ increases, the probability for getting a stop pulse after a start pulse has been registered decreases, and so the number of events recorded drops. We thus have a situation with many events near $\tau = 0$ and fewer at later times, which is fully compatible with the classical results in eqns 6.11 and 6.12.

This simple discussion should make it apparent that sometimes the photon picture concurs with the classical results and sometimes it does not. The key point relates to the time intervals between the photons in the light beam; that is, whether the photons come in bunches or whether they are regularly spread out. This naturally leads us to the concepts of bunched and antibunched light, which is the subject of the next section.

6.5 Photon bunching and antibunching

In Section 5.4 we introduced a threefold classification of light according to whether the statistics were sub-Poissonian, Poissonian, or super–Poissonian. We now make a different threefold classification according to the second-order correlation function $g^{(2)}(\tau)$. The classification is based on the value of $g^{(2)}(0)$ and proceeds as follows:

- **bunched light**: $g^{(2)}(0) > 1$,
- **coherent light**: $g^{(2)}(0) = 1$,
- **antibunched light**: $g^{(2)}(0) < 1$.

This point is summarized in Table 6.2. A comparison of Tables 6.1 and 6.2 makes us realize that bunched and coherent light are compatible with the classical results, but not antibunched light. Antibunched light has no classical counterpart and is thus a purely quantum optical phenomenon.

Figure 6.6 is a simplistic attempt to illustrate the difference between the three different types of light in terms of the photons streams. The

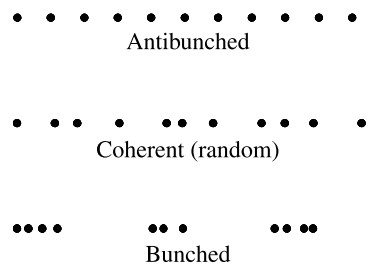

Fig. 6.6 Comparison of the photon streams for antibunched light, coherent light, and bunched light. For the case of coherent light, the Poissonian photon statistics correspond to random time intervals between the photons.

Table 6.2 Classification of light according to the photon time intervals. Antibunched light is a purely quantum state with no classical equivalent: classical light must have $g^{(2)}(0) \geq 1$.

Classical description	Photon stream	$g^{(2)}(0)$
Chaotic	Bunched	>1
Coherent	Random	1
None	Antibunched	<1

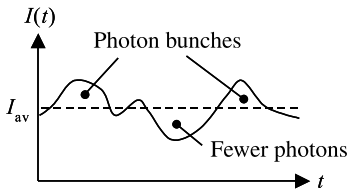

Fig. 6.7 Link between the classical intensity fluctuations about the average intensity I_{av} and photon bunching in a chaotic source. The photon bunches coincide with the high-intensity fluctuations.

reference point is the case where the time intervals between the photons are random. On either side of this we have the case where the photons spread out with regular time intervals between them, or where they clump together in bunches. These three cases correspond to coherent, antibunched, and bunched light, respectively. In what follows below, we explore the properties of each of these three types of light in more detail, starting with coherent light.

6.5.1 Coherent light

We have seen in Section 6.3 that perfectly coherent light has $g^{(2)}(\tau) = 1$ for all values of τ including $\tau = 0$. It thus provides a convenient reference for classifying other types of light.

In Section 5.3 we found that perfectly coherent light has Poissonian photon statistics, with random time intervals between the photons. This implies that the probability of obtaining a stop pulse is the same for all values of τ. We can thus interpret the fact that coherent light has $g^{(2)}(\tau) = 1$ for all values of τ (cf. eqn 6.13 and Fig. 6.4) as a manifestation of the randomness of the Poissonian photon statistics.

6.5.2 Bunched light

The tendency for photons to bunch together may be considered to be a manifestation of the fact that they are bosons.

Bunched light is defined as light with $g^{(2)}(0) > 1$. As the name suggests, it consists of a stream of photons with the photons all clumped together in bunches. This means that if we detect a photon at time $t = 0$, there is a higher probability of detecting another photon at short times than at long times. Hence we expect $g^{(2)}(\tau)$ to be larger for small values of τ than for longer ones, so that $g^{(2)}(0) > g^{(2)}(\infty)$.

We have seen in Section 6.3 that classical light must satisfy eqns 6.11 and 6.12. It is apparent that bunched light satisfies these conditions and is therefore consistent with a classical interpretation. It is also apparent from Table 6.1 that chaotic light (whether Gaussian or Lorentzian) also satisfies these conditions. The chaotic light from a discharge lamp is therefore bunched.

The link between photon bunching and chaotic light is illustrated schematically in Fig. 6.7, which shows the classical fluctuations in the

light intensity as a function of time. Since the photon number is proportional to the instantaneous intensity, there will be more photons in the time intervals that correspond to high-intensity fluctuations and fewer in the low-intensity fluctuations. The photon bunches will therefore coincide with the high-intensity fluctuations.

6.5.3 Antibunched light

In antibunched light the photons come out with regular gaps between them, rather than with a random spacing. This is illustrated schematically in Fig. 6.6. If the flow of photons is regular, then there will be long time intervals between observing photon counting events. In this case, the probability of getting a photon on D2 after detecting one on D1 is small for small values of τ and then increases with τ. Hence antibunched light has

$$g^{(2)}(0) < g^{(2)}(\tau),$$
$$g^{(2)}(0) < 1. \tag{6.17}$$

This is in violation of eqns 6.11 and 6.12 which apply to classical light. Hence the observation of photon antibunching is a purely quantum effect with no classical counterpart. The $g^{(2)}(\tau)$ functions for two possible forms of antibunched light are sketched schematically in Fig. 6.8. The key point is that $g^{(2)}(0)$ is less than unity.

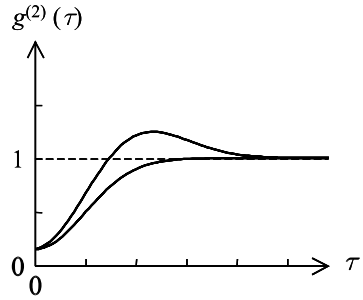

Fig. 6.8 Second-order correlation function $g^{(2)}(\tau)$ for two possible forms of antibunched light.

In Section 5.6 we studied the properties sub–Poissonian light and concluded that it, like antibunched light, is also a clear signature of the quantum nature of light. The question then arises whether photon antibunching and sub-Poissonian photon statistics are different manifestations of the same quantum optical phenomenon. This point has been considered by Zou and Mandel and the answer is negative. At the same time, it is apparent that a regular photon stream such as that illustrated in Fig. 6.6 will have sub-Poissonian photon statistics. Thus although the two phenomena are not identical, it will frequently be the case that nonclassical light will show both photon antibunching and sub-Poissonian photon statistics at the same time.

See X. T. Zou, and L., Mandel, *Phys. Rev A* **41**, 475 (1990).

6.6 Experimental demonstrations of photon antibunching

We have seen above that the observation of photon antibunching is a clear proof of the quantum nature of light. The first successful demonstration of photon antibunching was made by Kimble *et al.* in 1977 using the light emitted by sodium atoms. The basic principle of an antibunching experiment is to isolate an *individual* emitting species (i.e. an individual atom, molecule, quantum dot, or colour centre) and regulate the rate at which the photons are emitted by fluorescence. This is done by shining a laser onto the emissive species to excite it, and then waiting

See H. J. Kimble, M. Dagenais, and L. Mandel, *Phys. Rev. Lett.* **39**, 691 (1977).

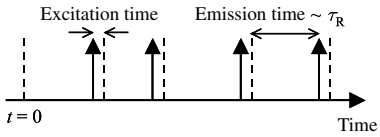

Fig. 6.9 Schematic representation of the photon emission sequence from a single atom excited by an intense laser. The dashed lines indicate the times at which the atom is promoted to the excited state, while the arrows indicate the photon emission events. τ_R is the radiative lifetime of the excited state.

Note that it is important to filter the light so that only a single transition wavelength is detected. See the discussion of Fig. 6.12(b) below.

for the photon to be emitted. Once a photon has been emitted, it will take a time approximately equal to the radiative lifetime of the transition, namely τ_R, before the next photon can be emitted. This leaves long time gaps between the photons, and so we have antibunched light.

We can understand this process in more detail by referring to Fig. 6.9, which shows a schematic representation of the photon emission sequence from a single atom. Let us suppose that the atom is promoted to an excited state at time $t = 0$, as indicated by the dashed line. The emission probability of the transition dictates that the average time to emit the photon is equal to τ_R. Once the photon has been emitted, the atom can be re-excited by the laser, which will only require a short amount of time if a high-power laser is used. The atom can then emit another photon after a time $\sim \tau_R$, at which point the excitation–emission cycle can start again. Since spontaneous emission is a probabilistic process, the emission time will not be the same for each cycle, which means that the stream of photons will not be exactly regular. However, it is clear that the probability for the emission of two photons with a time separation $\ll \tau_R$ will be very small. There will therefore be very few events when both the start and stop detectors of the HBT correlator in Fig. 6.5 fire simultaneously, and so we shall have $g^{(2)}(0) \approx 0$.

At this point we might legitimately ask why we do not observe the same antibunching effects from a conventional light source such as a discharge lamp. The point is that the antibunching effects are only observed if we look at the light from a *single* atom. The excitation–emission cycle shown in Fig. 6.9 is taking place for each individual atom in a discharge

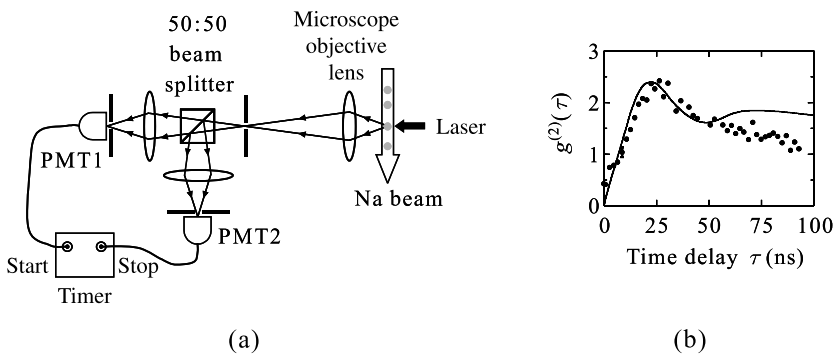

Fig. 6.10 (a) Schematic representation of the apparatus used to observe photon antibunching from the $3^2P_{3/2} \rightarrow 3^2S_{1/2}$ transition at 589.0 nm in atomic sodium. The sodium atomic beam was excited with a resonant laser and the fluorescence from one or two atoms only was collected with a microscope objective lens. The light beam was then split by a 50 : 50 beam splitter and detected with two photomultiplier tubes (PMT1 and PMT2) in a HBT arrangement. (b) Second-order correlation function $g^{(2)}(\tau)$ extracted from the data. The solid line is a theoretical fit calculated for a single atom. (After H.J. Kimble, M. Dagenais, and L. Mandel, *Phys. Rev. Lett.*, **39**, 691 (1977), © American Physical Society, reproduced with permission.)

lamp, but the light that is emitted originates from millions of atoms. The excitation and emission processes for the different atoms are statistically independent, and so they all emit at different times. This produces the photon bunches that are observed in the light emitted from a large number of atoms in a discharge lamp.

Figure 6.10(a) gives a schematic diagram of the apparatus used by Kimble *et al.* in 1977 to observe photon antibunching from a sodium atom. The sodium atomic beam was excited with a laser and the fluorescence from the $3^2P_{3/2} \rightarrow 3^2S_{1/2}$ transition at 589.0 nm was collected with a microscope objective lens. By using a very dilute beam, it was possible to arrange that, on average, no more than one or two atoms were able to contribute to the collected fluorescence at the same time. The fluorescence was then divided by a 50 : 50 beam splitter and detected by two photomultipliers in a HBT arrangement. The results obtained are shown in Fig. 6.10(b). Very few events were recorded near $\tau = 0$, and then $g^{(2)}(\tau)$ increased on a time-scale comparable to the radiative lifetime, namely 16 ns. At large time delays $g^{(2)}(\tau)$ decayed towards the asymptotic value of unity. The measured value of $g^{(2)}(0)$ was 0.4, which was a clear indication that the light was antibunched.

From a theoretical standpoint, it was expected that $g^{(2)}(0)$ should be zero if only a single atom was being observed. (See solid curve in Fig. 6.10(b).) The reason why the experimental value was larger was related to the experimental difficulty in arranging that only one atom should be in the field of view of the collecting lens at any one time. In practice, there were sometimes two or more, and this increased the value of $g^{(2)}(0)$ because of the possibility that two photons originating from different atoms should impinge on the beam splitter at the same time, and subsequently produce an event at $\tau = 0$ if the two photons go to different detectors. (See Exercise 6.11.)

In the years following Kimble *et al.*'s work, much progress has been made in atomic antibunching experiments. For example, antibunching has now been demonstrated from a one-atom laser in the strong coupling regime of cavity quantum electrodynamics (QED). Moreover, antibunching has also been observed from many other types of light emitters, including a number of solid-state sources, such as:

- fluorescent dye molecules doped in a glass or crystal;
- semiconductor quantum dots;
- colour centres in diamonds.

As an example, Fig. 6.11 shows the $g^{(2)}(\tau)$ function measured for an individual semiconductor quantum dot at cryogenic temperatures. The sample consisted of an InAs quantum dot embedded within a GaAs microdisk as shown in Fig. 6.11(a). The purpose of the microdisk was to increase the collection efficiency of the photons emitted by the quantum dot. The quantum dot was excited with continuous light at 760 nm and the photons emitted across the band gap of the quantum dot at 937.7 nm

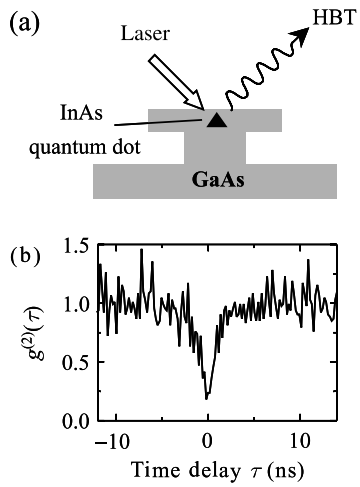

Fig. 6.11 (a) Excitation of an individual InAs quantum dot embedded within a GaAs microdisk structure using a continuous Ti:sapphire laser at 760 nm. The photons emitted from the quantum dot at 937.7 nm were detected with a HBT arrangement similar to the one shown in Fig. 6.5. (b) Second-order correlation function $g^{(2)}(\tau)$ measured for the quantum dots at 4 K. (After P. Michler *et al.*, *Science* **290**, 2282 (2000), ©AAAS, reprinted with permission.)

See Section 10.4 for a discussion of strong coupling effects in cavity QED, and Appendix D for an overview of the properties of semiconductor quantum dots. The strongly coupled one-atom laser is reported by J. McKeever *et al.* in *Nature* **425**, 268 (2003). For further information on antibunched light from solid-state sources, see, for example: Th. Basché *et al.*, *Phys. Rev. Lett.* **69**, 1516 (1992); P. Michler *et al.*, *Nature* **406**, 968 (2000); A. Beveratos *et al.*, *Phys. Rev. A*, **64**, 061802 (2001).

were detected with a HBT correlator. The results obtained at 4 K are shown in Fig. 6.11(b). The observed $g^{(2)}(0)$ value of ~ 0.2 is a clear signature of photon antibunching.

In this experiment the main reason why $g^{(2)}(0)$ was not zero was related to the finite response time of the detector, namely 0.42 ns. With a radiative lifetime of 2.2 ns, there was a significant probability of emission by 0.42 ns, and this contributed to the signal recorded at $\tau = 0$ because the detectors could not discriminate between these two times. (See Exercise 6.9.) Note that this is a different situation from the sodium experiment shown in Fig. 6.10, where the lifetime was much longer. At the same time, the quantum dots were fixed in the crystal lattice and so there was no chance that more than one emissive species could contribute to the fluorescence, as was the case for the atomic beam.

6.7 Single-photon sources

Single-photon sources are also required for the scheme proposed in Knill *et al.* (2001) to perform efficient quantum computation with linear optics. This scheme contrasts with the work described in Chapter 13 in which the quantum information is stored in atoms or ions and the photons are only used to manipulate the quantum bits.

An application of the techniques for the generation of antibunched light is the development of a triggered **single-photon source**. As explained in Section 12.5, these sources are needed to improve the security in quantum cryptography experiments. The basic idea of a single-photon source is that the source should emit exactly one photon in response to a trigger pulse, which can be either electrical or optical. The operating principle is shown in Fig. 6.12. The source consists of a single emissive species (say an atom), and the trigger pulse excites the atom to an upper excited state, as shown in Fig. 6.12(a). The atom then emits a cascade of photons as it relaxes to the ground state. Since the photons have different wavelengths, it is possible to select the photon from a particular transition by filtering the fluorescence. There will only ever be one photon emitted from a specific transition in each cascade.

Consider now the timing of the photons emitted by this process. An intense trigger pulse will rapidly promote an electron to the excited state,

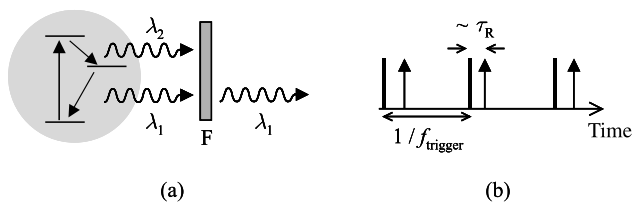

Fig. 6.12 Excitation–emission cycle from a single atom in response to trigger pulses. (a) The atom emits a cascade of photons of different wavelengths as it relaxes, but by using a suitable filter (F), only one of them is selected. (b) Schematic representation of the photon emission sequence. Trigger pulses are indicated by the thick lines, while the arrows indicate the photon emission events, which occur at a time roughly equal to the radiative lifetime (τ_R) after the trigger pulses. When the pulse separation $1/f_{trigger}$ is significantly longer than τ_R, the photon stream is controlled by the trigger pulse sequence.

and the atom will emit exactly one photon after a time roughly equal to the radiative lifetime τ_R, as shown schematically in Fig. 6.12(b). No more photons can be emitted until the next trigger pulse arrives, when the process repeats itself. The time separation of the trigger pulses is determined by the frequency f_{trigger} at which the trigger source operates. If the time separation between the pulses is significantly longer than τ_R, the trigger pulses control the separation of the photons in the fluorescence. We thus have a source that emits exactly one photon of a particular wavelength whenever a trigger pulse is applied.

The easiest way to make a triggered single-photon source is to use an optical trigger from a suitable laser. However, in the long run it will be important to develop electrically triggered devices. Figure 6.13 illustrates one such implementation incorporating a single quantum dot as the light-emitting species. The device consisted of a GaAs light emitting diode (LED) with a layer of InAs quantum dots inserted within the active region. The quantum dots were excited by a programmed sequence of

Experiments describing a molecular single-photon source are reported by B. Lounis and W.E. Moerner, *Nature* **407**, 491 (2000). The equivalent experiments for colour centres in diamond are described in C. Kurtsiefer *et al.*, *Phys. Rev. Lett.*, **85**, 290 (2000). The first two results on quantum dot single-photon sources are described in P. Michler *et al.*, *Science* **290**, 2282 (2000) and C. Santori *et al.*, *Phys. Rev. Lett.* **86** 1502 (2001). All of these experiments use optical trigger pulses. The electrically driven single-photon source discussed here was reported by Z. Yuan *et al.*, *Science* **295**, 102–5 (2002).

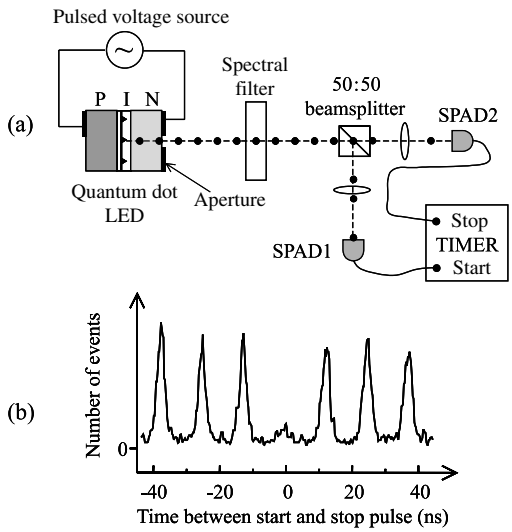

Fig. 6.13 An electrically driven triggered single-photon source. (a) Schematic representation of the experiment. The source consisted of a quantum dot LED driven by a pulsed voltage source. A single layer of InAs quantum dots was inserted within the intrinsic (I) region of a GaAs P-I-N diode. The quantum dots emitted light pulses in response to the pulsed voltage source. The photons were transmitted through the transparent N-type GaAs layer above the quantum dots and then through a small aperture in the metallic top contact. This aperture was small enough that it selected the light from only a few quantum dots, which emitted at different wavelengths due to their differing sizes. A spectrometer was then used as a spectral filter to select the emission at 889.3 nm from an individual quantum dot. The statistics of these selected photons were measured using a HBT arrangement with fast SPADs as the detectors. (b) Results obtained for a pulse repetition rate of 80 MHz with the device at 5 K. The count rate showed peaks corresponding to the pulse train period of 12.5 ns. The absence of a peak at zero time interval indicates the low probability that the quantum dot emitted two photons of the same wavelength at the same time. (After Z. Yuan *et al.*, Science **295**, 102 (2002), ©AAAS, reprinted with permission.)

current pulses produced by a pulsed voltage source. The current pulse injected electrons and holes into the device, and the quantum dots then emitted a light pulse in response to each trigger pulse. An aperture in the top contact ensured that the light from only a few of the InAs quantum dots was collected. The emission wavelength of a quantum dot depends on its size, which varies from dot to dot due to statistical fluctuations related to the crystal growth. Hence the wavelength varied slightly from dot to dot, which allowed the light emitted from a particular emission line of an individual quantum dot to be selected by using a spectrometer as a spectral filter. In these circumstances, we expect the light to be antibunched, as demonstrated previously in Fig. 6.11.

Figure 6.13(b) presents the results of the HBT experiment performed on the filtered light emitted from the device using fast single-photon avalanche photodiodes (SPADs) as the detectors. These results can be understood as follows. Let us suppose a photon strikes SPAD1 and generates a trigger pulse to start the timer. The timer will then measure the time that elapses before another photon strikes SPAD2 and generates the stop signal. This second photon may have come from the same light pulse as the first one, or from a different one. In the former case, we will record an event near $\tau = 0$. In the latter case, we will record an event near $\tau = m/f_{\text{trigger}}$, where m is an integer and $f_{\text{trigger}} = 80$ MHz is the frequency of the trigger pulse sequence. Hence the histogram of events will show peaks separated by 12.5 ns in these experiments. The key feature of the results is the very small number of events recorded near $\tau = 0$. This indicates that the source is emitting only one photon in each pulse, because there would have to be at least two photons in the pulse in order to register events at $\tau = 0$. In other words, we must have achieved a single-photon light source.

The results shown in Fig. 6.13 represent a substantial step towards the development of a convenient source for generating single photons on demand. At the present time, the main experimental difficulties that have to be overcome before these single-photon sources find more widespread applications is the low overall quantum efficiency and the operating temperature, which was 5 K for the data presented in Fig. 6.13.

An elegant experiment demonstrating the wave–particle duality of light using a single-photon source is shown schematically in Fig. 6.14. The light from a quantum dot single-photon source was divided equally with a 50 : 50 beam splitter and sent either to a Michelson interferometer or to a HBT experiment. The data from the HBT experiment was collected simultaneously with the fringe pattern from the interferometer. Clear interference fringes demonstrating the wave nature of light were observed at the same time as antibunching, which is a purely photon (i.e. particle) effect. Although it is clear that the individual photons go either to the interferometer or to the HBT experiment, it is very unlikely that the presence of one piece of apparatus can affect the results of the other. Therefore, the simultaneous observation of fringes and antibunching during a data collection run is a good demonstration of the wave–particle duality of light.

The principles of the Michelson interferometer are explained in Section 2.2.2.

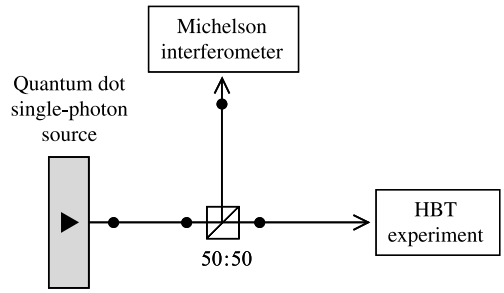

Fig. 6.14 Demonstration of the wave–particle duality of light using a quantum dot single-photon source. A 50 : 50 beam splitter sends half the photons to a Michelson interferometer and the other half to a HBT experiment. Interference fringes were observed at the same time as antibunching. Details of the experiment may be found in Zwiller *et al.*, *Phys. Rev. B* **69**, 165307 (2004).

Further reading

Introductory descriptions of the stellar intensity interferometer may be found in many standard optics texts, for example Brooker (2003), Hecht (2002), or Smith and King (2000). A more detailed discussion may be found in Hanbury Brown (1974).

The classical interpretation of the second-order correlation function is covered very rigorously in Mandel and Wolf (1995), while many useful insights are also to be found in Loudon (2000). Both of these texts develop the equivalent quantum theory in depth. Teich and Saleh (1990) give an introduction to antibunched light, and a more detailed account may be found in Teich and Saleh (1988). Thorn (2004) describes an undergraduate experiment to demonstrate photon antibunching.

An introductory account of single-photon sources has been given by Grangier and Abram (2003), and a collection of papers on the sources and their applications may be found in Grangier *et al.* (2004). There have now been many reports of the generation of antibunched light by semiconductor quantum dots. A review may be found in Michler (2003), while Petroff (2001) gives details of the techniques used to grow the dots.

Exercises

(6.1) Consider the fringe pattern from light of wavelength λ produced in a Young's double-slit experiment from a source of finite size D. Let the distance from the source to the slits be L ($L \gg D$) and the separation of the slits be d. Show that the dark fringes from the centre of the source coincide with the bright fringes from the edges when $D/L = \lambda/d$.

(6.2) In the HBT experiment shown in Fig. 6.2, a high-pass filter was inserted between the detector and the amplifier to remove the DC component of the photocurrent and the low-frequency electrical noise.

(a) Design a simple circuit employing a capacitor and a resistor to act as the filter.

(b) Calculate the value of the resistor to use for a cut-off frequency of 1 MHz if the capacitor has a capacitance of 1 nF.

(6.3) In this exercise we will prove eqn 6.11 by following the approach in Loudon (2000).

(a) By considering the quantity $(x(t_1) - x(t_2))^2$, where $x(t)$ is a real number, prove Cauchy's inequality:

$$x(t_1)^2 + x(t_2)^2 \geq 2x(t_1)x(t_2).$$

(b) Cauchy's inequality applied to $I(t)$ gives:

$$I(t_1)^2 + I(t_2)^2 \geq 2I(t_1)I(t_2).$$

Consider the quantity:

$$\left(\sum_{i=1}^{N} I(t_i)\right)^2 = (I(t_1) + I(t_2) + \cdots + I(t_N))^2 = \sum_{i=1}^{N}\sum_{j=1}^{N} I(t_i)I(t_j).$$

Apply Cauchy's inequality to each of the cross-terms to show that:

$$\left(\sum_{i=1}^{N} I(t_i)\right)^2 \leq N\sum_{i=1}^{N} I(t_i)^2.$$

(c) We define the average of the intensity as the mean of a large number of measurements made at different times according to:

$$\langle I(t)\rangle = \frac{1}{N}\sum_{i=1}^{N} I(t_i).$$

The average of $I(t)^2$ is defined in the same way:

$$\langle I(t)^2\rangle = \frac{1}{N}\sum_{i=1}^{N} I(t_i)^2.$$

Substitute these definitions into the result of part (b) to show that:

$$\langle I(t)\rangle^2 \leq \langle I(t)^2\rangle.$$

Hence derive eqn 6.11.

(6.4) The purpose of this exercise is to establish eqn 6.12 by a method similar to the one used in the previous exercise.

(a) Use Cauchy's inequality to show that:

$$\sum_{i=1}^{N} I(t_i)I(t_i+\tau) \leq \frac{1}{2}\sum_{i=1}^{N}(I(t_i)^2 + I(t_i+\tau)^2).$$

(b) Explain why, in any stationary light source (i.e. one in which the averages do not vary with time), we expect:

$$\sum_i I(t_i)^2 = \sum_i I(t_i+\tau)^2.$$

(c) The argument of part (b) allows us to rewrite the result of part (a) in the form:

$$\sum_{i=1}^{N} I(t_i)I(t_i+\tau) \leq \sum_{i=1}^{N} I(t_i)^2.$$

Following the definition of time averages given in part (c) of the previous exercise, we can write:

$$\langle I(t)I(t+\tau)\rangle = \frac{1}{N}\sum_{i=1}^{N} I(t_i)I(t_i+\tau).$$

Use this definition to show that:

$$\langle I(t)I(t+\tau)\rangle \leq \langle I(t)^2\rangle.$$

Hence derive eqn 6.12.

(6.5) Show that, in terms of the intensity fluctuations defined by $\Delta I(t) = (I(t) - \langle I(t)\rangle)$, the second-order correlation function $g^{(2)}(\tau)$ may be written in the form:

$$g^{(2)}(\tau) = 1 + \frac{\langle \Delta I(t)\Delta I(t+\tau)\rangle}{\langle I(t)\rangle\langle I(t+\tau)\rangle}.$$

Hence prove that $g^{(2)}(0) \geq 1$ for classical light.

(6.6) Calculate the values of $g^{(2)}(0)$ for a monochromatic light wave with a square wave intensity modulation of $\pm 20\%$.

(6.7) The 632.8 nm line of a neon discharge lamp is Doppler-broadened with a linewidth of 1.5 GHz. Sketch the second-order correlation function $g^{(2)}(\tau)$ for τ in the range 0–1 ns.

(6.8) The 546.1 nm line of a pressure-broadened mercury lamp has a line width of 0.001 nm. Sketch the second-order correlation function $g^{(2)}(\tau)$ for τ in the range 0–1 ns.

(6.9) (a) A single atom is irradiated with a powerful beam from a continuous wave laser which can promote it to an excited state with a radiative lifetime of τ_{R}. On the assumption that the excitation time is negligibly small, calculate the probability that the atom emits two photons in a time T.

(b) In a Hanbury Brown–Twiss (HBT) experiment, single-photon counting detectors with a response time of τ_{D} are connected to the start and stop inputs of a timer. The finite response time of the detectors implies that two events separated in time by $\leq \tau_{\mathrm{D}}$ will be registered as simultaneous. Use this fact, together with the result of part (a), to estimate the value of $g^{(2)}(0)$ that would be expected in a HBT experiment using detectors of response times τ_{D} on a single atom with a radiative lifetime of τ_{R}.

(6.10) Discuss the dependence of $g^{(2)}(\tau)$ on the power of the exciting laser for an antibunching experiment such as that shown in Fig. 6.11 when using detectors of response time τ_{D} as in the previous question.

(6.11) A source emits a regular train of pulses, each containing exactly two photons. What value of $g^{(2)}(0)$ would be expected?

(6.12) A quantum dot with a radiative lifetime of 1 ns is used to make a single-photon source. What is the maximum photon bit rate that can be achieved?

(6.13) A source emits a train of single photons with exactly regular time intervals between them. Sketch the $g^{(2)}(\tau)$ function that would be expected:

(a) when the time interval between the photons is very much larger than the response time τ_{D} of the detector;

(b) when the time interval is very much smaller than τ_{D}.